Journal of the Optical Society of America B
OPTICAL PHYSICS

Polarization dependence of interferences inside rubidium atomic vapor governing microwave vector E-field metrology

Harish Singh Rawat,[1,2] Satya Kesh Dubey,[1,2,*] and Vijay Narain Ojha[2]

[1] Academy of Scientific and Innovative Research (AcSIR), Ghaziabad-201002, India
[2] CSIR-National Physical Laboratory, Dr. K. S. Krishnan Marg, New Delhi-110012, India
*Corresponding author: dubeysk@nplindia.org

Received 4 June 2019; revised 21 September 2019; accepted 21 October 2019; posted 21 October 2019 (Doc. ID 369324); published 26 November 2019

The atom-based metrology technique has been widely accepted because of the SI traceability and dependence only on the physical constants rather than on any artefact. The presented work explains the dependence of the probe absorption on the polarization of the driving fields in the new atom-based spectroscopic technique for microwave electrometry. This work explains the nature of decays between different pathways when the fields are not only π or σ polarized but also at an arbitrary angle between the two orientations. It has been shown that when any of the lasers is linearly polarized at an arbitrary angle $0 < \theta_{p,c} < \pm\pi/2$ to the quantization axis, the observation of the absorption from a correct direction becomes extremely important. The findings in this work can be utilized in the correct determination of the polarization of the incident microwave field along with the E-field amplitude measurement. Further, a challenge has been discussed when the radio frequency (RF) field is weak and cannot give the distinguished separation in the absorption peak. It has been shown that the sensitivity of the sensor can be increased in this case by detuning the RF from the on-resonance frequency.

https://doi.org/10.1364/JOSAB.36.003547

1. INTRODUCTION

Quantum coherence has been a rigorous topic of study in recent years because it has provided us with legitimate explanations of the many optical phenomena in atom–photon interaction physics. The interaction between light and medium modifies the medium's optical characteristics, which are explored by many groups. The refractive index of the medium can be manipulated to obtain cross-phase modulation [1,2] or photon switching [3]. The quantum coherence between atomic levels can make the medium transparent for a particular frequency of light known as electromagnetically induced transparency (EIT) [4,5]. Also, the coherences can be manipulated to observe electromagnetically induced absorption (EIA) [6,7]. Detailed study of the coherences helped us in distinguishing a similar looking phenomenon known as Autler–Townes splitting (ATS) [8] from EIT. These three phenomena named EIT, ATS, and EIA are utilized in the field of precision metrology by using the properties of Rydberg atoms in alkali vapors. With time, many groups have presented different mathematical techniques to understand the interferences. We have shown the nature of resonances occurring inside an atom by the resonant pole method in our previous work [9], Abi-Salloum [10] and Anisimov *et al.* [11] have explained EIT and ATS through a dressed-state picture, and Lu *et al.* [12] applied the Fourier-transform-based technique to distinguish between the two. However, all these techniques have not considered the polarization mismatch between the driving fields and have considered the fields to be co-polarized.

Recently, the International Bureau of Weights and Measures (BIPM) has decided to redefine all the basic SI units in terms of the physical constants that describe the natural world. Various laboratories across the world have shown promising results by applying precision atomic spectroscopy to find the new primary standard for various fields, such as length, gravity, time, frequency, and magnetic field [13]. The motivation behind the rigorous study of the discussed technique is that it provides SI unit traceability with extreme precision by exploiting the known atomic and molecular characteristics of atoms. Recently, numerous experimental studies have reported the feasibility of the atom-based metrology technique for RF E-field amplitude [14–19] as well. Some of the challenges and effects on the sensitivity in atom-based RF E-field sensing are given in [20]. The huge transition dipole moment between the Rydberg states gives great sensitivity to the microwave E-field and has proven to sense the E-field with higher accuracy and sensitivity than the conventional E-field probes currently in use.

In this paper, we have shown that the atom-based microwave electrometry technique not only provides precise E-field amplitude measurement but also can be used for the microwave polarization measurement. This vector E-field measurement utilizes the hyperfine structure of the atom, and the selection rule of transitions helps in understanding the nature of interferences occurring between the available pathways for the decay. In this work, the microwave frequency is considered to be 133.65 GHz, staying in line with the various new technologies in a variety of industries and other sectors. With the increase in demand of high bandwidth and data rate, the emerging technologies in the fields of wireless communication, atmospheric monitoring, and bio-medical imaging are bound to shift to frequencies above 100 GHz and further to the terahertz bands. Therefore in the near future it would become an absolute necessity to establish the calibration techniques of microwave E-field measurement with SI traceability at high frequencies where the calibration probes used at present fail.

2. PHYSICAL MODEL

An atomic vapor cell of ^{87}Rb under the simultaneous influence of two optical fields and one RF field is considered for this work; the orientation of three interacting fields and a vapor cell is depicted in Fig. 1. The lasers are considered to propagate in the z direction with a red laser (780 nm) propagating in the $+z$ direction and a blue laser (483.924 nm) propagating in $-z$ direction. Microwave is considered to travel in an orthogonal direction to the laser propagation, the $+y$ direction. The weak red laser probing the atomic ensemble is observed for the response and will be referred to as "probe" throughout this work. The probe laser with E-field $\vec{E}_p = \epsilon_p(\hat{x}\cos\theta_p + \hat{y}\sin\theta_p)e^{-i(\omega_p t - k_p z)} + \text{c.c.}$ is tuned to the D_2 line of ^{87}Rb and couples ground state $|1\rangle \to 5S_{1/2}$ $(F = 2,\ m_f = \pm 2)$ to $|2\rangle \to 5P_{3/2}$ $(F = 3,\ m_f = \pm 3)$. Another optical field, a strong blue laser with E-field $\vec{E}_c = \epsilon_c(\hat{x}\cos\theta_c + \hat{y}\sin\theta_c)e^{-i(\omega_c t + k_c z)} + \text{c.c.}$, is used to pump the atom into the excited state [couples states $|2\rangle \to 5P_{3/2}$ $(F = 3,\ m_f = \pm 3)$ and $|3\rangle \to 26D_{5/2}$ $(F = 4,\ m_f = \pm 4)$] and will be referred to as "control" hereafter. The third field (RF) traveling in the orthogonal direction to optical fields with E-field $\vec{E}_\mu = \epsilon_\mu(\hat{x}\sin\phi_\mu + \hat{z}\cos\phi_\mu)e^{-i(\omega_\mu t - k_\mu y)} + \text{c.c.}$ couples $|3\rangle \to 26D_{5/2}$ $(F = 4,\ m_f = \pm 4)$ to $|4\rangle \to 27P_{3/2}$ $(F = 3,\ m_f = \pm 3)$. All the field expressions are expressed in general form, where $\epsilon_{p,c,\mu}$, $\omega_{p,c,\mu}$, and $k_{p,c,\mu}$ represent the slowly varying envelope, frequency, and propagation constant for probe, control, and RF, respectively. The angles $\theta_{p,c}$ and ϕ_μ are self-explanatory and are shown in Fig. 1. The Rabi frequencies of the probe, control, and RF controlled transitions can be written as $\Omega_p = \vec{d}_{12}.\{\epsilon_p(\hat{x}\cos\theta_p + \hat{y}\sin\theta_p)\}/\hbar$, $\Omega_c = \vec{d}_{23}.\{\epsilon_c(\hat{x}\cos\theta_c + \hat{y}\sin\theta_c)\}/\hbar$, and $\Omega_\mu = \vec{d}_{34}.\{\epsilon_\mu(\hat{x}\sin\phi_\mu + \hat{z}\cos\phi_\mu)\}/\hbar$, where $\vec{d}_{jk}$ represents the transition electric-dipole element between the energy levels $|j\rangle$ and $|k\rangle$.

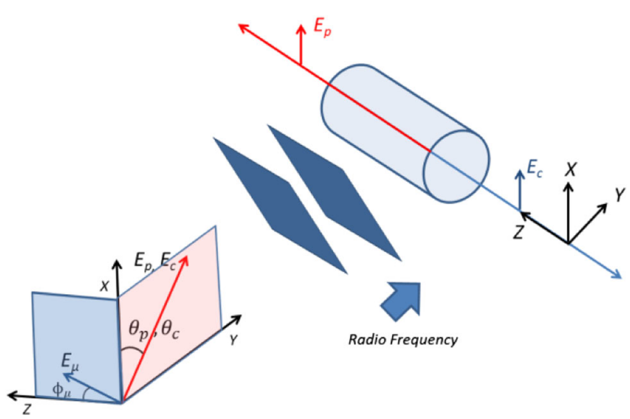

Fig. 1. Representational diagram of the atom–photon interaction based technique for microwave amplitude measurement. The two optical fields propagate in either direction along the z axis, and RF propagates in the y direction. In the presented case, the E-field vectors of lasers ($\vec{E}_p$, $\vec{E}_c$) make angles θ_p and θ_c with the x axis in the xy plane. The RF E-field vector ($\vec{E}_\mu$) makes an angle ϕ_{rf} with the direction of propagation of lasers in the xz plane.

The total Hamiltonian for this system under dipole approximation by keeping the atomic level $|1\rangle$ as the reference point for all energy levels with zero energy at $|1\rangle$ can be expressed as

$$\hat{H} = \hbar\,(0|1\rangle\langle 1| + \omega_{21}|2\rangle\langle 2| + \omega_{31}|3\rangle\langle 3| + \omega_{41}|4\rangle\langle 4|) - \left[\vec{d}_{12}|2\rangle\langle 1| + \text{H.C.}\right].\vec{E}_p - \left[\vec{d}_{23}|3\rangle\langle 2| + \text{H.C.}\right].\vec{E}_c - \left[\vec{d}_{34}|4\rangle\langle 3| + \text{H.C.}\right].\vec{E}_\mu, \quad (1)$$

where $\hbar\omega_{ji}$ is the energy difference between the energy levels $|j\rangle$ and $|i\rangle$, and $\vec{d}_{ij}$ is the dipole moment of corresponding transitions, $\vec{d}_{ij} = \langle i|\hat{d}|j\rangle$ for transitions $|i\rangle \to |j\rangle$. The evolution of the system can be described by the density matrix equations of motion and is given by

$$\dot{\rho} = -\frac{i}{\hbar}[H, \rho] - \frac{1}{2}\{\Gamma, \rho\}, \quad (2)$$

where $\{\Gamma, \rho\} = \Gamma\rho + \rho\Gamma$ and Γ is the relaxation matrix. The density matrix equations for the matrix elements are obtained by considering rotating wave approximation by neglecting the highly oscillating terms and are expressed as

$$\begin{aligned}
\dot{\rho}_{11} &= \gamma_{21}\rho_{22} - i\Omega_p\rho_{12} + i\Omega_p^*\rho_{21},\\
\dot{\rho}_{22} &= \gamma_{32}\rho_{33} - \gamma_{21}\rho_{22} - i\Omega_c\rho_{23} + i\Omega_c^*\rho_{32} + i\Omega_p\rho_{12} - i\Omega_p^*\rho_{21},\\
\dot{\rho}_{33} &= \gamma_{43}\rho_{44} - \gamma_{32}\rho_{33} - i\Omega_\mu\rho_{34} + i\Omega_\mu^*\rho_{43} + i\Omega_c\rho_{23} - i\Omega_c^*\rho_{32},\\
\dot{\rho}_{44} &= -\gamma_{43}\rho_{44} + i\Omega_\mu\rho_{34} - i\Omega_\mu^*\rho_{43},\\
\dot{\rho}_{21} &= d_1\rho_{21} + i\Omega_p(\rho_{11} - \rho_{22}) + i\Omega_c^*\rho_{31},\\
\dot{\rho}_{31} &= d_2\rho_{31} + i\Omega_\mu^*\rho_{41} + i\Omega_c\rho_{21} + i\Omega_p\rho_{32},\\
\dot{\rho}_{41} &= d_3\rho_{41} + i\Omega_\mu^*\rho_{31} + i\Omega_p^*\rho_{42},\\
\dot{\rho}_{32} &= (i\Delta_c - \Gamma_{32})\rho_{32} + i\Omega_c(\rho_{22} - \rho_{33}) + i\Omega_\mu^*\rho_{42} + i\Omega_p^*\rho_{31},\\
\dot{\rho}_{43} &= \left(i\Delta_\mu - \Gamma_{43}\right)\rho_{43} + i\Omega_\mu(\rho_{33} - \rho_{44}) + i - \Omega_c^*\rho_{42},
\end{aligned} \quad (3)$$

where $\Delta_p = \omega_p - \omega_{21}$, $\Delta_c = \omega_c - \omega_{32}$, and $\Delta_\mu = \omega_\mu - \omega_{43}$ are the detunings of the transition probe, control, and microwave field for $|1\rangle \rightarrow |2\rangle$, $|2\rangle \rightarrow |3\rangle$, and $|3\rangle \rightarrow |4\rangle$, respectively. γ_{ji} is the spontaneous emission rate from level $|i\rangle \rightarrow |j\rangle$, and Γ_{ji} is the de-phasing rate of coherence between the levels $|i\rangle \rightarrow |j\rangle$ and is given by $\Gamma_{ji} = \frac{1}{2}\sum_k(\gamma_{ki} + \gamma_{kj}) + \gamma_{\text{col.}}$, where $\gamma_{\text{col.}}$ is the collisional decay rate.

The off-diagonal element responsible for the probe absorption can be obtained by solving Eq. (3) under a steady state condition by considering weak probe approximation and is given by

$$\rho_{21} = -\frac{i\Omega_p\left(\Omega_\mu^2 + d_2 d_3\right)}{d_1\Omega_\mu^2 + d_3\Omega_c^2 + d_1 d_2 d_3}, \quad \textbf{(4)}$$

where d_1, d_2, and d_3 are complex detunings and are given by $(i\Delta_p - \Gamma_{21})$, $\{i(\Delta_p + \Delta_c) - \Gamma_{31}\}$, and $\{i(\Delta_p + \Delta_c + \Delta_\mu) - \Gamma_{41}\}$, respectively. To determine the response of the atomic medium to the applied fields, we monitor the susceptibility χ. The real part of the susceptibility gives the dispersion, and the imaginary part gives the absorption of the probe field in the medium. The susceptibility is defined as

$$\chi = \frac{3Nc^2}{2\omega_p^3}\rho_{21}, \quad \textbf{(5)}$$

where N is the number density of the atomic medium. The imaginary part of χ is monitored in this work for different values of all the system parameters.

3. RESULTS

A. Polarization Dependence of EIT

The role of the E-field vectors of all three driving fields plays a crucial role in the nature of the interference pattern occurring inside the atomic system. The system was investigated first by keeping the microwave switched off and the probe and coupling lasers linearly polarized and parallel to each other, i.e., $\hat{x}$ polarized. Other parameters are $\Gamma_{21} = 2\pi 6.065 \times 10^6$, $\Gamma_{43} = \Gamma_{32} = 2\pi 1.2 \times 10^3$, and $\Gamma_{41} = 2\pi 3.1 \times 10^3$. The quantization axis in this work is considered to be in the $\hat{x}$ direction. The selection rules for the radiative decay create coherences between the states. The π-polarized transitions govern the system, and the electron transitions experience a three-level system giving EIT due to the creation of a dark state in the system and are shown in Fig. 2(a) (black, dashed curve). Figure 2(b) showcases the energy level diagram for the π-polarized transitions in the three-level system. The $5S_{1/2}|2, \pm 2\rangle_x \rightarrow 5P_{3/2}|3, \pm 2\rangle_x \rightarrow 26D_{5/2}|i, \pm m_j\rangle_x$ transitions couple together, and EIT is observed in the $\hat{x}$ direction, where i represents the hyperfine level, and m_j represents the degenerate sublevel where j can take values $-i$ to i. The orientation of transitions as per the selection rule when the control laser is $+\sigma$ polarized is shown in Fig. 2(c). The solid and dashed lines represent π and σ transitions throughout this paper. One can clearly notice the one photon transition in the $\hat{x}$ direction resulting in the blue curve in Fig. 2(a). In this work, the single F states of the states $5S_{1/2}$ and $5P_{3/2}$ are considered as the hyperfine splittings can be easily resolved with 6.8 GHz and

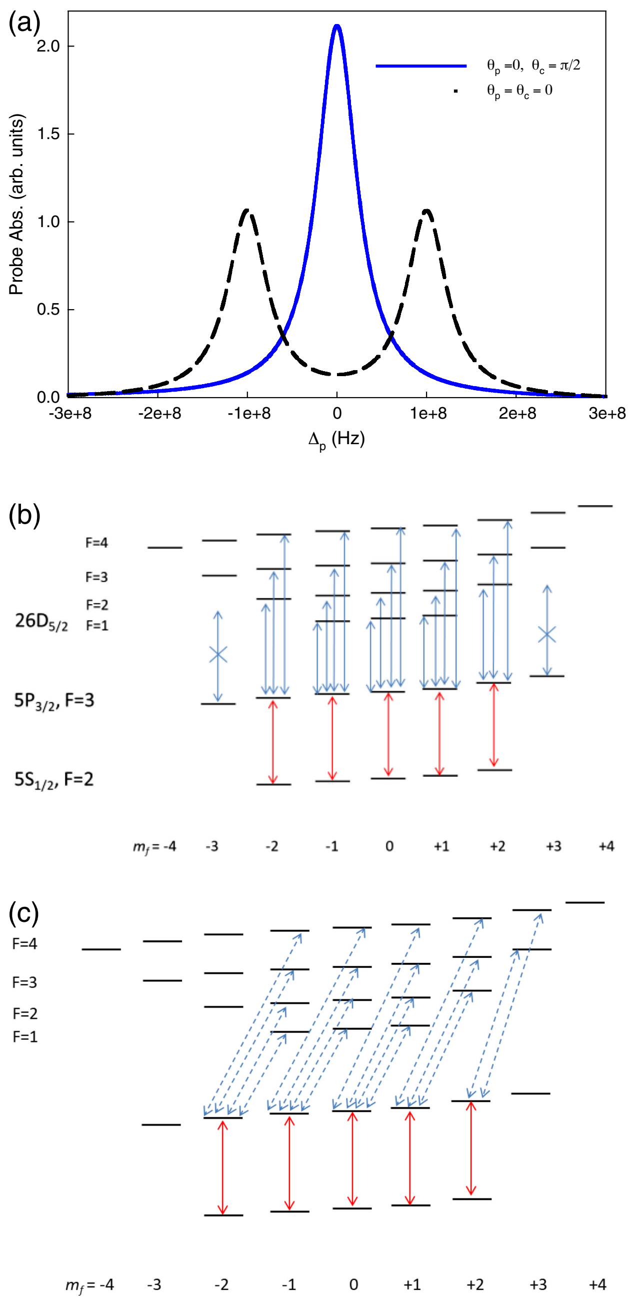

Fig. 2. (a) Probe absorption spectrum as a function of laser polarizations. EIT is observed when both lasers are linearly and co-polarized (black); otherwise two-photon transition could not occur in π transitions and hence there would be no EIT (blue). (b) Possible π transitions when the fields are polarized along the quantization axis inducing three-level Rydberg EIT [black in (a)]. (c) Possible transitions when control laser is $+\sigma$ polarized; since probe absorption is monitored in the $\hat{x}$ direction, we observe probe absorption in a two-level single photon transition [blue in (a)].

266 MHz, respectively. The other states are considered degenerate as the energy difference between the m_f levels is much easier to distinguish.

This behavior of coherences within the three-level ladder system is referred to as Rydberg EIT and is experimentally observed by [21]. Further, when any of the laser is relatively orthogonally polarized to the other one, no EIT is observed; the probe laser is absorbed [Fig. 2(a) (blue curve)]. This bolsters the fact that even if there are good conditions for EIT, a polarization mismatch prohibits the creation of a dark state. Our findings agree with the work conforming that EIT is dependent on the polarization of the driving fields [22–24].

B. Autler–Townes Splitting of EIT

The system is further investigated by projecting microwave (RF) onto the vapor cell along with the two optical fields. Both the lasers are $\hat{x}$ polarized, and RF is $\hat{z}$ polarized (in the direction of laser propagation), i.e., $\theta_p = \theta_c = 0$, $\emptyset_\mu = 0$. The microwave cannot couple the fourth state to the three-level Rydberg EIT via π polarized transitions. The system experiences EIT via three-state $5S_{1/2}|2, \pm 2\rangle_x \rightarrow 5P_{3/2}|3, \pm 2\rangle_x \rightarrow 26D_{5/2}|i, \pm m_j\rangle_x$ interference, shown by a green curve in Fig. 3(a). A similar result is experimentally obtained by Sedlacek *et al.* [25], where they have shown that the microwave can be used to couple or decouple the Rydberg states and RF polarization can be tuned to observe either EIT or the ATS of EIT.

Next, the microwave E-field vector is rotated in the right direction at the xz plane keeping the E-field vectors of both lasers $\hat{x}$ polarized; a third peak at the center of the EIT window is observed in the probe absorption spectrum. This is due to the creation of a bright state in the continuum by the perpendicular component of $\vec{E}_\mu$ allowing π transitions to occur by coupling the fourth state with Rydberg EIT making four-level $5S_{1/2}|2, \pm 2\rangle_x \rightarrow 5P_{3/2}|3, \pm 2\rangle_x \rightarrow 26D_{5/2}|i, \pm m_j\rangle_x \rightarrow 27P_{3/2}|k, \pm m_l\rangle_x$ transitions represented by solid straight lines in Fig. 3(c); i and k represent hyperfine levels, and m_j and m_l represent degenerate sublevels, where j and l can take values $-i$ to i and $-k$ to k, respectively. This bright state allows the photons to be reabsorbed, giving the split in the transparent window. Similar results where three-level EIT is changed to a four-level ATS due to the presence of the fourth state are validated experimentally in [25,26]. The other system parameters are the same as in Fig. 2. The red, blue, and pink curves displayed in Fig. 3(a) are for the cases in which $\emptyset_\mu = \pi/8, \pi/4$, and $\pi/2$ indicating the increase in dominance of π transitions with the increase in the polarization misalignment between the RF and laser E-field vectors. Figure 3(c) represents all the possible transitions between the energy states in the case being discussed, but as the probe absorption is observed only in the $\hat{x}$ direction, only the transitions shown by solid lines contribute. It can be easily inferred from simple vector rotation geometry that when $\vec{E}_\mu$ is rotated beyond $\pi/2$ the dominance of π transitions begins to reduce (reduction in central peak). If it is further rotated until $\emptyset_\mu = \pi$ (in the direction of control laser propagation), again EIT is observed conforming the elimination of π transitions, and the system is reduced to three-level EIT, displayed by the fifth curve (green) in Fig. 3(a).

C. Vector Microwave E-Field Sensing

It is understood now that it becomes essential to observe the probe absorption spectra parallel to the quantization axis in order to observe the substantial variations in the absorption spectrum with the respective variations in microwave field. This change in the absorption behavior with RF polarization can be

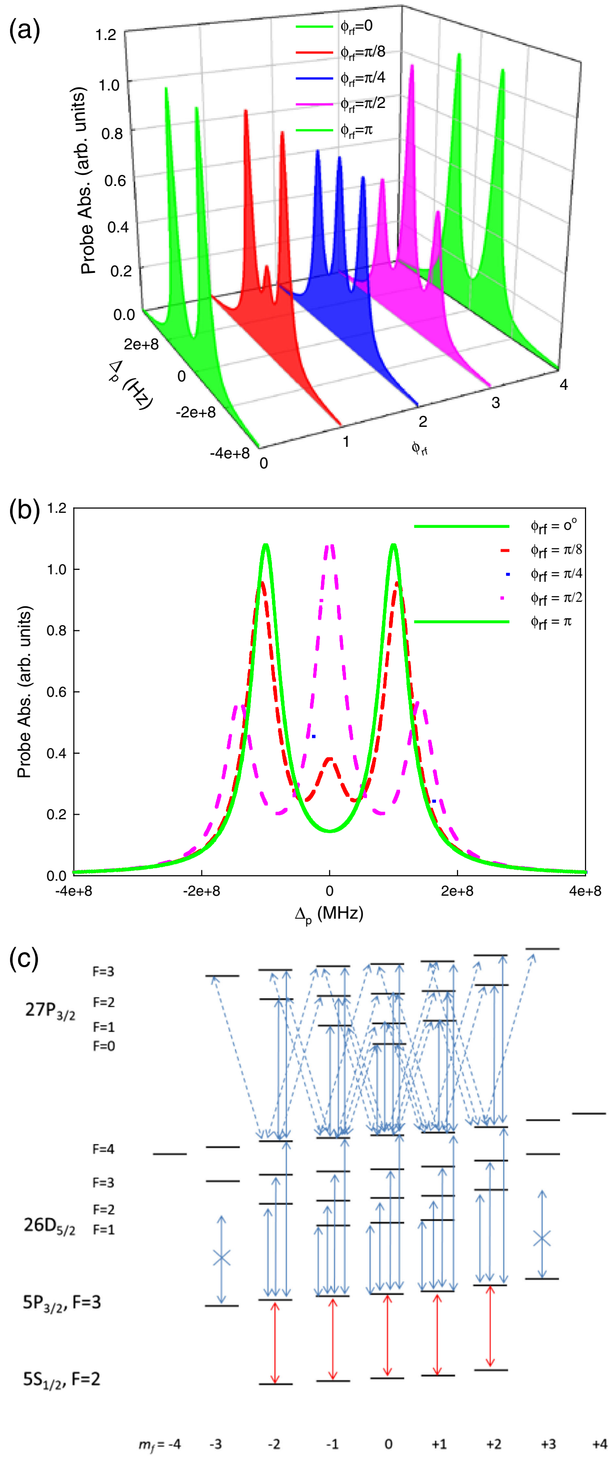

Fig. 3. (a) Probe absorption as a function of $\vec{E}_\mu$ orientation. The $\vec{E}_\mu$ is rotated in the xz plane, and the change in absorption is depicted for angles $\phi = 0, \pi/8, \pi/4, \pi/2$, and π by green, red, blue, pink, and green, respectively. (b) Two-dimensional view of (a). (c) All possible transitions when $\vec{E}_p$ and $\vec{E}_c$ are $\hat{x}$-polarized and $\vec{E}_\mu$ is rotated in the xz plane. Solid and dashed lines represent π and σ transitions, respectively.

used as an important tool in atom-based microwave metrology for its amplitude and vector electric field measurement. The splitting between the two absorption peaks is different for all the cases. The minor shift of the order of megahertz in the resonant curves is due to the coupling of multiple states by the parallel and perpendicular components of $\vec{E}_\mu$. Another reason can be the inhomogeneity of the microwaves inside the vapor cell, or the presence of a small amount of ionization. One may observe this from Fig. 3(b), which is a two-dimensional plot of Fig. 3(a). The difference between the absorption peaks helps in determining the RF E-field amplitude [15] and is given by

$$E_\mu = \Omega_\mu \frac{\hbar}{d_\mu} = 2\pi \Delta f \frac{\hbar}{d_\mu}. \quad (6)$$

Recently, various groups have studied and showed promising measurement results for high-frequency E-field metrology using the atom-based spectroscopy technique for microwave measurement. This method may replace the standard E-field probes for RF-infrared E-field measurement in the near future [20]. Our findings can be used as an extension to this technique for sensing the microwave vector E-field. For this, the change (rise of the third peak) in the absorption spectrum with the change in $\vec{E}_\mu$ orientation can be used as a very crucial and important tool in determining the microwave polarization vector.

Another interesting part of our finding is that EIT can also be obtained when the probe and control lasers are linearly polarized, and is in the direction of the RF propagation, i.e., $\theta_p = \theta_c = \pi/2$, and the probe absorption curve is the same as shown in Fig. 2(a). But in this condition the ATS of EIT cannot be achieved with the change in $\vec{E}_\mu$ vector direction because $\vec{E}_\mu$ cannot be in the direction of RF propagation and hence cannot interfere with optical field vectors. One may easily understand from Fig. 3(c) that once there is no transition and

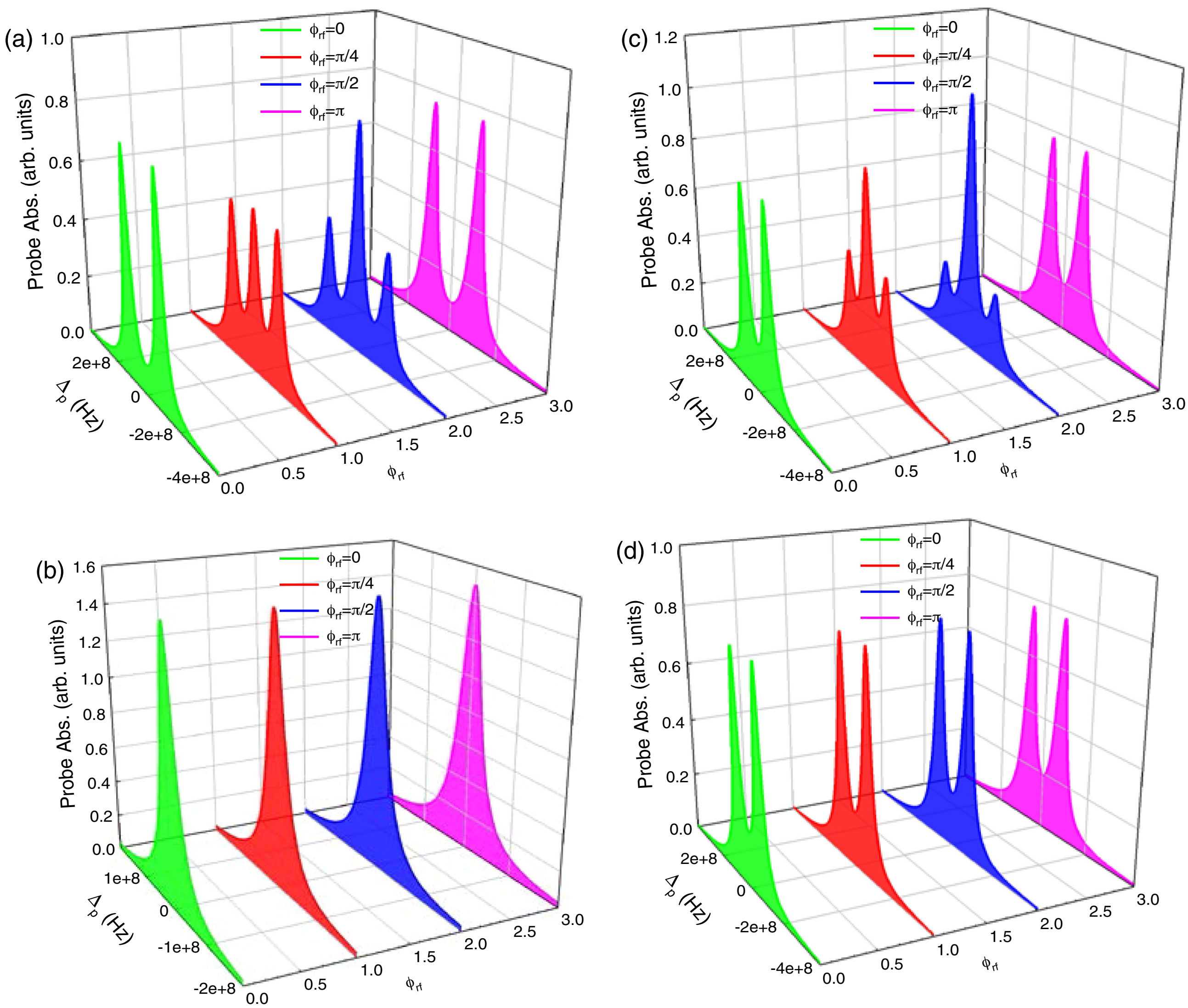

Fig. 4. (a) Probe absorption as a function of $\vec{E}_\mu$ orientation as observed in the $\hat{x}$ direction. The $\vec{E}_\mu$ is rotated in the xz plane, and the change in absorption is depicted for angles $\phi = 0, \pi/8, \pi/4, \pi/2$, and π by green, red, blue, pink, and green, respectively, for the case in which the control laser is $\hat{x}$-polarized and $\theta_p = \pi/4$. (b) Probe absorption when observed in the $\hat{y}$ direction. It appears to be absorbed in the two-level system due to the σ transitions due to the perpendicular component. (c) Probe absorption for the case in which both lasers are co-polarized and $\theta_p = \theta_c = \pi/4$ as observed in the $\hat{x}$ direction. (d) Probe absorption as observed in the $\hat{y}$ direction. The perpendicular components of both laser vectors give rise to σ transitions, and EIT is observed because of interferences via σ transitions in the three-level system.

hence interference between the $26D_{5/2}$ and $27P_{3/2}$ states in the $\hat{x}$ or $\hat{y}$ direction, the system experiences three-level EIT. The relaxations through σ transitions govern the system, and EIT can only be obtained when observed from the transverse direction. Thus one may infer from the discussion above that, for EIT to occur, both the lasers should be co-polarized, but for ATS of EIT to occur all the field vectors must lie on the same plane. This can pose difficulties and add certain uncertainties in the field of atom-based metrology for RF E-field sensing.

Also shown are the cases for variation in $\vec{E}_\mu$ when (i) only the probe laser is polarized at an angle $\pi/4$ to the quantization axis but not perpendicular to it, keeping control laser $\hat{x}$ polarized [Figs. 4(a) and 4(b)]. In this case the system experiences both the three-level and four-level transitions in the system. Figure 4(a) represents the case in which the response is observed in the $\hat{x}$ direction, and Fig. 4(b) represents the absorption observed from the $\hat{y}$ direction. The parallel component of $\vec{E}_p$ still contributes to the absorption, and ATS of EIT can be observed, whereas the perpendicular component gives rise to some σ transitions inside the system and gives absorption only as control laser driven transitions are still π polarized.

In the second case (ii) both the lasers are co-polarized at an angle $\pi/4$ to the quantization axis [Figs. 4(c) and 4(d)]; again when observed in the $\hat{x}$ direction the π transitions due to the microwave and the parallel components of both laser controlled transitions give ATS of EIT, whereas EIT is obtained when observed from the $\hat{y}$ direction. This is an important finding confirming the polarization dependence of the absorption on the differently polarized photons. The perpendicular components of both the laser coupled transitions give rise to σ transitions and experience three-level EIT. One should note that four-level interference cannot occur in the system in the $\hat{y}$ direction as the $\vec{E}_\mu$ can never be in the direction of propagation of the microwave field.

D. Weak RF Field Sensing

The RF E-field measurement becomes a bit complicated in the situation in which the RF field is weak. Even if there are correct conditions for the EIT to occur, the split in the absorption curve is so small that it becomes almost impossible to measure the Δf and hence E-field amplitude. The study presented in this work is further extended to analyze the weak RF field sensing. It has been found that the discussed technique can also sense weak RF fields by just varying the RF frequency. Kumar *et al.* [27] demonstrated the sensing of weak RF fields using Cs vapors by utilizing homodyne detection by using a Mach–Zehnder interferometer to cancel the readout noise. Simons *et al.* [28] suggested to increase the sensitivity of the microwave E-field sensing by studying the asymmetry and new separation between peaks induced in the EIT spectrum by the means of RF detuning. The detuned weak RF couples the near-resonant states and gives substantial variations in the probe absorption spectrum. Figure 5 shows the probe absorption as a function of RF detuning. The orientation of E-field vectors is $\theta_p = \theta_c = 0$, $\emptyset_\mu = \pi/2$, keeping all system parameters the same as in Fig. 2.

On the resonant RF frequency ATS of EIT is observed with two side-peaks of equal height. It has been observed that when the RF frequency is lower than the resonant frequency, the right peak is lowered with the increase in the left peak. The opposite is observed when the RF frequency is greater than the resonant frequency. Also, the peaks are shifted on either side with detuning of either direction. Our work yields results in good agreement with the fact given in [28], confirming that frequency can be detuned to increase the sensitivity of weak fields. One fact to remember is that the RF detuning method can only be performed when ATS of EIT is obtained—the condition discussed in Section 3.C.

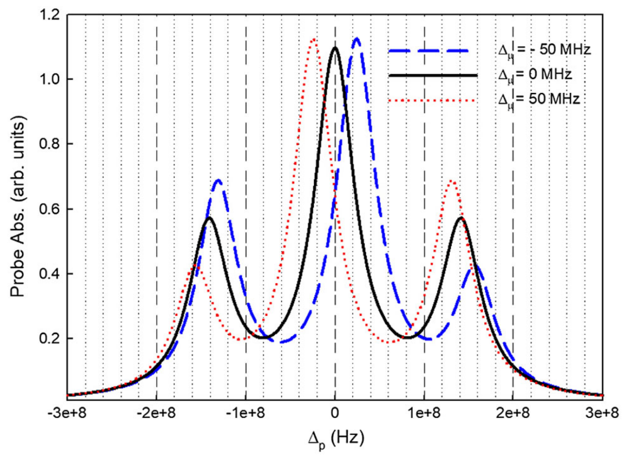

Fig. 5. Probe absorption as a function of microwave detuning. On the resonant RF frequency, ATS of EIT is observed with the two side-peaks of equal height. When the RF frequency is lower than the resonant frequency, the new splitting of the left curve is taken from the central curve (blue), and the opposite is done for higher frequency (red). The system parameters are $\theta_p = \theta_c = 0$, $\emptyset_\mu = \pi/2$, and all other parameters are the same as in Fig. 2.

The increased separation between the peaks when RF is detuned from resonance can be estimated by [28]

$$\Delta f_\delta = \sqrt{(\delta_{rf})^2 + (\Delta f_0)^2}, \quad (7)$$

where Δf_0 is the difference between peaks when the RF detuning is zero (the difference between black curves in Fig. 5); δ_{rf} is the RF detuning. One can observe from Fig. 5 that Δf_0 is 100 MHz (shown by a black arrow) and δ_{rf} can have values ± 50 MHz. The new spacing between the peaks as per the expression (7) would be 111.80 MHz, which can be cross verified by the separation of the left (right) peak from central one shown by blue (red) in Fig. 5 for -50 MHz ($+50$ MHz). The major and minor ticks in the result represent the difference of 100 and 20 MHz on the x axis. The FWHM of the peaks is considered to depict the separation between them. Recently this dependency of the asymmetry and separation between the curves has been utilized by many groups to achieve quantum communication using a similar measurement setup [29–31] in which a message signal is modulated with RF and demodulated from the changes in absorption spectrum of the probe conforming the reliability of the atom–photon interaction physics behind this spectroscopic microwave metrology technique.

4. CONCLUSION

This paper presents a theoretical study of the atom-based spectroscopic technique for microwave E-field measurement. It is demonstrated that for a three-level Rydberg EIT to occur, both the lasers should be co-polarized. If any of the laser is orthogonally polarized to the other, no EIT is observed. It has been also shown that the probe absorption responds very sensitively to the orientation of microwave E-field vector $\vec{E}_\mu$. A minute change in the orientation of $\vec{E}_\mu$ creates a substantial change in the behavior of the third peak at the middle of the EIT window. The findings in the presented work can be utilized for the determination of the vector E-field measurement as well.

Also, it has been shown that it is essential for an observer to observe the probe absorption via a correct axis. One may not observe EIT or ATS of EIT even under optimal conditions for it to occur if not observed from the direction in which the quantization axis lies. In addition, it has been also shown that we can detect weak microwave signals as well, using the same technique by just detuning the microwave signal in either direction. This slight detuning gives distinguishable asymmetry and new separation between the peaks in the probe absorption, which is easier to measure and which would be hard to measure in weak EIT. The presented work can be utilized in the determination of the polarization and amplitude of the microwave E-field in the Rydberg-atom-based metrology technique. Also it can be utilized in microwave communication via a sensor based on Rydberg atoms.

Funding. Science and Engineering Research Board (DST/SSK/SERB-CII-Fell/2014).

Acknowledgment. The authors are thankful to the Science and Engineering Research Board (SERB), Department of Science and Technology (DST), Government of India, and Confederation of Indian Industry (CII) for the Prime Minister Fellowship for Doctoral Research. The authors are also thankful to Rohde & Schwarz India Pvt. Ltd. for funding and participating in the Prime Minister Fellowship.

REFERENCES

1. H. Schmidt and A. Imamoglu, "Giant Kerr nonlinearities obtained by electromagnetically induced transparency," Opt. Lett. **21**, 1936–1938 (2008).
2. H. Schmidt and A. Imamoglu, "High-speed properties of a phase-modulation scheme based on electromagnetically induced transparency," Opt. Lett. **23**, 1007–1009 (2008).
3. S. E. Harris and Y. Yamamoto, "Photon switching by quantum interference," Phys. Rev. Lett. **81**, 3611–3614 (1998).
4. M. Fleischhauer, A. Imamoglu, and J. P. Marangos, "Electromagnetically induced transparency: optics in coherent media," Rev. Mod. Phys. **77**, 633–673 (2005).
5. J. P. Marangos, "Electromagnetically induced transparency," J. Mod. Opt. **45**, 471–503 (1998).
6. A. V. Taichenachev, A. M. Tumaikin, and V. I. Yudin, "Electromagnetically induced absorption in a four-state system," Phys. Rev. A **61**, 3–6 (2002).
7. A. M. Akulshin, S. Barreiro, and A. Lezama, "Electromagnetically induced absorption and transparency due to resonant two-field excitation of quasidegenerate levels in Rb vapor," Phys. Rev. A **57**, 2996–3002 (1998).
8. C. H. Autler and S. H. Townes, "Stark effect in rapidly varying fields," Phys. Rev. **100**, 703–722 (1955).
9. H. S. Rawat, S. K. Dubey, and V. N. Ojha, "Distinction between double electromagnetically induced transparency and double Autler–Townes splitting in RF-driven four-level ladder ^{87}Rb atomic vapor," J. Phys. B **51**, 155401 (2018).
10. T. Y. Abi-Salloum, "Electromagnetically induced transparency and Autler-Townes splitting: two similar but distinct phenomena in two categories of three-level atomic systems," Phys. Rev. A **81**, 053836 (2010).
11. P. M. Anisimov, J. P. Dowling, and B. C. Sanders, "Objectively discerning Autler-Townes splitting from electromagnetically induced transparency," Phys. Rev. Lett. **107**, 21–24 (2011).
12. X. Lu, X. Miao, J. Bai, L. Pei, M. Wang, Y. Gao, L. A. Wu, P. Fu, R. Wang, and Z. Zuo, "Transition from Autler-Townes splitting to electromagnetically induced transparency based on the dynamics of decaying dressed states," J. Phys. B **48**, 055003 (2015).
13. K. Cox, V. I. Yudin, A. V. Taichenachev, I. Novikova, and E. E. Mikhailov, "Measurements of the magnetic field vector using multiple electromagnetically induced transparency resonances in Rb vapor," Phys. Rev. A **83**, 015801 (2011).
14. J. A. Sedlacek, A. Schwettmann, H. Kübler, R. Löw, T. Pfau, and J. P. Shaffer, "Microwave electrometry with Rydberg atoms in a vapour cell using bright atomic resonances," Nat. Phys. **8**, 819–824 (2012).
15. C. L. Holloway, J. A. Gordon, M. T. Simons, D. A. Anderson, A. Schwarzkopf, S. A. Miller, N. Thaicharoen, and G. Raithel, "Broadband Rydberg atom-based electric-field probe: from self-calibrated measurements to sub-wavelength imaging," IEEE Trans. Antennas Propag. **62**, 6169–6182 (2014).
16. D. A. Anderson, S. A. Miller, G. Raithel, J. A. Gordon, M. L. Butler, and C. L. Holloway, "Optical measurements of strong microwave fields with Rydberg atoms in a vapor cell," Phys. Rev. Appl. **3**, 1–7 (2016).
17. C. L. Holloway, M. T. Simons, J. A. Gordon, A. Dienstfrey, D. A. Anderson, and G. Raithel, "Electric field metrology for SI traceability: systematic measurement uncertainties in electromagnetically induced transparency in atomic vapor," J. Appl. Phys. **121**, 233106 (2017).
18. S. Kumar, H. Fan, H. Kübler, A. J. Jahangiri, and J. P. Shaffer, "Rydberg-atom based radio-frequency electrometry using frequency modulation spectroscopy in room temperature vapor cells," Opt. Express **25**, 8625–8637 (2017).
19. M. T. Simons, J. A. Gordon, and C. L. Holloway, "Simultaneous use of Cs and Rb Rydberg atoms for dipole moment assessment and RF electric field measurements via electromagnetically induced transparency," J. Appl. Phys. **120**, 123103 (2016).
20. H. Fan, S. Kumar, J. Sedlacek, H. Kübler, S. Karimkashi, and J. P. Shaffer, "Atom based RF electric field sensing," J. Phys. B **48**, 202001 (2015).
21. S. Sevinçli, C. Ates, T. Pohl, H. Schempp, C. S. Hofmann, G. Günter, T. Amthor, M. Weidemüller, J. D. Pritchard, D. Maxwell, and A. Gauguet, "Quantum interference in interacting three-level Rydberg gases: coherent population trapping and electromagnetically induced transparency," J. Phys. B **44**, 184018 (2011).
22. D. McGloin, M. H. Dunn, and D. J. Fulton, "Polarization effects in electromagnetically induced transparency," Phys. Rev. A **62**, 053802 (2000).
23. Y.-W. Chen, C.-W. Lin, Y.-C. Chen, and I. A. Yu, "Quantization axes in coherent two-field spectroscopy," J. Opt. Soc. Am. B **19**, 1917–1921 (2002).
24. Y.-C. Chen, C.-W. Lin, and I. A. Yu, "Role of degenerate Zeeman levels in electromagnetically induced transparency," Phys. Rev. A **61**, 053805 (2000).
25. J. A. Sedlacek, A. Schwettmann, H. Kübler, and J. P. Shaffer, "Atom-based vector microwave electrometry using rubidium Rydberg atoms in a vapor cell," Phys. Rev. Lett. **111**, 1–5 (2013).
26. C. L. Holloway, M. T. Simons, J. A. Gordon, P. F. Wilson, C. M. Cooke, D. A. Anderson, and G. Raithel, "Atom-based RF electric field metrology: from self-calibrated measurements to subwavelength and near-field imaging," IEEE Trans. Electromagn. Compat. **59**, 717–728 (2017).

27. S. Kumar, H. Fan, H. Kübler, J. Sheng, and J. P. Shaffer, "Atom-based sensing of weak radio frequency electric fields using homodyne readout," Sci. Rep. **7**, 1–10 (2017).
28. M. T. Simons, J. A. Gordon, C. L. Holloway, D. A. Anderson, S. A. Miller, and G. Raithel, "Using frequency detuning to improve the sensitivity of electric field measurements via electromagnetically induced transparency and Autler-Townes splitting in Rydberg atoms," Appl. Phys. Lett. **108**, 174101 (2016).
29. Z. Song, W. Zhang, H. Liu, X. Liu, H. Zou, J. Zhang, and J. Qu, "The credibility of Rydberg atom based digital communication over a continuously tunable radio-frequency carrier," arXiv:1808.10839 (2018).
30. Y. Jiao, X. Han, J. Fan, G. Raithel, J. Zhao, and S. Jia, "Atom-based quantum receiver for amplitude-and frequency-modulated baseband signals in high-frequency radio communication," arXiv:1804.07044 (2018).
31. C. L. Holloway, M. T. Simons, A. H. Haddab, C. J. Williams, and M. W. Holloway, "Quantum physics meets music: a "real-time" guitar recording using Rydberg-atoms and electromagnetically induced transparency," AIP Adv. **9**, 065110 (2019).